

Tunable metal-insulator transition and superconductivity in twisted bilayer graphene

Wanying Chen,¹ Yonghuan Chu,¹ Tongyun Huang,¹ and Tianxing Ma^{1,*}

¹Department of Physics, Beijing Normal University, Beijing 100875, China

Motivated by recent experimental studies that have found signatures of a correlated insulator phase and tuning superconductivity in twisted bilayer graphene, we study the temperature-dependent conductivity, the spin correlation and the superconducting pairing correlation within a two-orbital Hubbard model on an emergent honeycomb lattice. Evaluation of the temperature dependence of the conductivity demonstrates that there is a metal-insulator transition, and the Mott phase at strong coupling is accompanied by antiferromagnetic order. The electronic correlation drives a $d + id$ superconducting pairing to be dominant over a wide filling region. All of the dc conductivity, the spin correlation and the superconductivity are suppressed as the interlayer coupling strength increases, and the critical U_c for metal-insulator transition is also reduced. Our intensive numerical results reveal that the TBG should be a uniquely tunable platform for exploring correlated states.

Introduction: In accordance with recent experiments on twisted bilayer graphene (TBG), the arresting phenomena containing novel phases, unconventional superconductivity as well as a Mott-like insulator behavior have been discovered in such a magical two-dimensional system which demonstrates the importance of correlations effect[1, 2], and most recently, a tuning superconductivity is induced by varying the interlayer spacing with hydrostatic pressure, which sparked more intense interest in TBG as it maybe a uniquely tunable platform for exploring correlated states[3].

With two layers of graphene twisted at a narrow range of particular magic angle in TBG, its band structure becomes nearly flat, and as a result, the Fermi velocity drops to zero in the vicinity of the Fermi energy. Being interpreted as a correlated Mott insulator at half-filling[1], this system is doped with a few extra charge carriers and then it changes from the initial insulator to a superconductor[2], which shares a striking similar trend as that in doped cuprates[4], heavy-fermion[5], iron-based[6] and organic superconductors[7]. Consequently, this has been the subject of intense studies since the discovery of high-temperature superconductors [8], which may shed light on several long-standing problems encompassing the understanding of unconventional superconductivity, and even more prove to be a significant step in the searching for room-temperature superconductors.

Substantial theoretical effort has gone into this filed[9–42], and many possibilities of the exotic electronic structures further reflect the fact that TBG can be a realistic platform for various kinds of largely unknown physics. However, it is difficult to identify an effective low-energy model to deal with the strong correlation effects in TBG, as the moiré pattern in TBG with small twist angles requires a very large system size, more than 10, 000 atoms in one unit cell, which makes an usual first-principles electronic structure calculation is almost impossible. Constructed from Wannier orbitals that extend over the size of supercells, a two-orbital

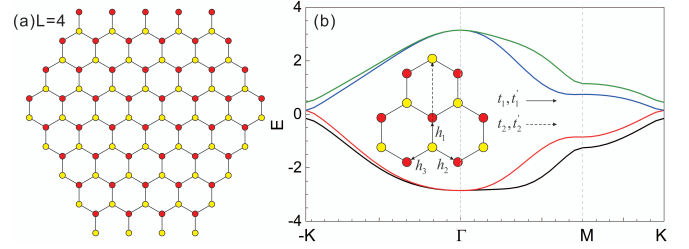


FIG. 1. (Color online) (a) The geometry of TBG for the effective model[17, 18] with $L = 4$; (b) the band structure of the corresponding tight-binding model. The insert shows the definition of hoppings.

Hubbard model sketched in Fig.1 is proposed to capture the electronic structure of narrow minibands and the effect of Coulomb interaction in TBG, and the centers of these Wannier orbitals form an emergent honeycomb lattice[17, 18]. This model, has been verified by explicit numerical calculations[25, 29], and provide us an opportunity to explore the rich physics in TBG by the un-biased numerical method, which is the most reliable way to establish the phase diagram in the system where the strong correlation effect dominates.

The metal-insulator transition, itself is one of the most fundamental and yet profound physical phenomenon of quantum mechanics, while our understanding of interaction-driven metal-insulator transitions still remains rather controversial because strongly correlated systems are hard to solve using both analytical and numerical methods[43]. In this paper, within the two-orbital Hubbard model on an emergent honeycomb lattice, we perform a quantum Monte carlo study of the metal-insulator transition in TBG. Calculations of the current-current correlation function show that repulsion between electrons can significantly reduce the conductivity, and at low temperatures change the system from conducting behavior to insulating behavior. After making a careful finite size scaling analysis, we demonstrate that the metal-Insulator

transition is associated with the presence of the antiferromagnetic long-range order. Inspired by the experimental results of varying the interlayer spacing with hydrostatic pressure, a tuning metal-insulator transition and superconductivity in TBG is proposed by studying the interlayer coupling strength dependent spin correlation, conductivity and superconducting pairing correlation.

Model and methods: In the effective model, the tight-binding part H_{tb} mainly contains the intralayer hoppings H_0 , and H_1 and H_2 are also introduced into H_{tb} to further break the SU(4) and SU(1) symmetries [17, 18]. The detailed H_{tb} can be written as follows,

$$\begin{aligned} H_{tb} &= H_0 + H_1 + H_2, \\ H_0 &= \sum_{\langle ij \rangle} t_1 [\mathbf{c}_i^\dagger \cdot \mathbf{c}_j + h.c.] + \sum_{\langle ij \rangle'} t_2 [\mathbf{c}_i^\dagger \cdot \mathbf{c}_j + H.c.], \\ H_1 &= \sum_{\langle ij \rangle'} t'_2 [(\mathbf{c}_i^\dagger \times \mathbf{c}_j)_z + H.c.] \\ &= -i \sum_{\langle ij \rangle'} t'_2 (c_{i+}^\dagger c_{j+} - c_{i-}^\dagger c_{j-}) + H.c., \\ H_2 &= \sum_{\langle ij \rangle} t'_1 [\mathbf{c}_i^\dagger \cdot \parallel e_{ij}^\parallel \cdot \mathbf{c}_j - \mathbf{c}_i^\dagger \cdot e_{ij}^\perp \cdot \mathbf{c}_j + H.c.], \end{aligned} \quad (1)$$

where $\mathbf{c}_i = (c_{i,x}, c_{i,y})^T$ with $c_{i,x(y)}$ annihilates an electron with $p_{x(y)}$ -orbital at site i . t_1 and t_2 are the hopping amplitude between nearest-neighbor (NN) and fifth-NN sites, respectively, the sketch of hoppings is shown in the insert of Fig. 1(b). The chiral basis $c_\pm = (c_x \pm ic_y)/\sqrt{2}$ is associated with $p_x \pm ip_y$ orbitals. $e_{ij}^{\parallel,\perp}$ denotes in-plane unit vectors in the direction parallel and perpendicular to the NN bond $\langle ij \rangle$, respectively. The on-site Coulomb interaction part is written as

$$H_U = U \sum_{i,m} \mathbf{n}_{im\uparrow} \mathbf{n}_{im\downarrow}, \quad (2)$$

where m is the $p_{x(y)}$ orbitals, and $\mathbf{n}_{im\sigma} = \mathbf{c}_{im\sigma}^\dagger \cdot \mathbf{c}_{im\sigma}$. This model provides a theoretical framework for studying correlated electron phenomena and superconductivity in TBG. In our following simulations, the system we performed is sketched in Fig. 1(a) with periodic boundary conditions, and we take t_1 as the unit. The parameters we used are $t_1 = 1.0$, $t'_1 = 0.1$, $t_2 = 0.025$, and $t'_2 = 0.1$, which are taken from that of Refs.[17, 18]. Within this set of parameters, one can see that the band structure in Fig. 1(b) is degenerate with finite t'_1 except Γ and K points, where electrons are localized.

Our simulations are mostly performed on lattice of $L=4$, and the total number of lattice sites is $N_s=2 \times 2 \times 3L^2$, in which the first 2 indicating two orbits, and the second 2 means two interpenetrating triangular sublattices with hexagonal shape such that it preserves most geometric symmetries of graphene[44–46]. To make the finite-size scaling analysis, lattices with $L=3,4,5,6$

are also simulated. The basic strategy of the finite temperature determinant Monte Carlo (DQMC) method is to express the partition function as a high-dimensional integral over a set of random auxiliary fields. The integral is then accomplished by Monte Carlo techniques. In our simulations, 8 000 sweeps were used to equilibrate the system, and an additional 30 000~240 000 sweeps were then made, each of which generated a measurement. These measurements were split into ten bins which provide the basis of coarse-grain averages and errors were estimated based on standard deviations from the average. In order to assess our results and their accuracy with respect to the infamous sign problem as the particle-hole symmetry is broken, a very careful analysis on the average of sign is illustrated.

To explore the phase transitions between the metal and insulator behaviors, we compute the T -dependent DC conductivity, which is calculated from the wave vector \mathbf{q} - and imaginary time τ -dependent current-current correlation function[47] $\Lambda_{xx}(\mathbf{q}, \tau)$,

$$\sigma_{dc}(T) = \frac{\beta^2}{\pi} \Lambda_{xx}(\mathbf{q} = 0, \tau = \frac{\beta}{2}) \quad (3)$$

where $\Lambda_{xx}(\mathbf{q}, \tau) = \langle \hat{j}_x(\mathbf{q}, \tau) \hat{j}_x(-\mathbf{q}, 0) \rangle$, $\beta = 1/T$, $\hat{j}_x(\mathbf{q}, \tau)$ is the (\mathbf{q}, τ) -dependent current operator in x direction. Eq.3 has been employed for metal-insulator transitions in Hubbard model in many works and it has already proved its validity[47–49].

In order to examine how the system evolves with the variation of the magnetic order, we study the antiferromagnetic (AFM) spin structure factor

$$S_{AFM} = \frac{1}{N_s} \langle [\sum_{lr} (\hat{S}_{lar}^z - \hat{S}_{lbr}^z)]^2 \rangle, \quad (4)$$

which indicates the onset of long-range AFM order if $\lim_{N_s \rightarrow \infty} (S_{AFM}/N_s) > 0$. Here, $\hat{S}_{lar}^z (\hat{S}_{lbr}^z)$ is the z component spin operator on A (B) sublattice of layer l . S_{AFM} for different interactions are calculated on lattices with $L = 3, 4, 5, 6$, and are extrapolated to the thermodynamic limit using polynomial functions in $1/\sqrt{N_s}$.

Results and discussion— Firstly, we examine the AFM spin structure factor behaviors versus inverse temperature β for different lattice size L and interaction strength U . Here we use $t_1 = 1.0$, $t'_1 = 0.1$, $t_2 = 0.025$, and $t'_2 = 0.1$. In the following, we fix $t_1 = 1.0$, $t_2 = 0.025$, and may vary $t'_1 = t'_2$ to explore the tunable physics inspired by the experimental results where the interlayer spacing is varied with hydrostatic pressure. From Fig. 2(a), we can see that the AFM spin structure factor increases as the lattice size increases slightly as $U \geq 3.5$, and it increases evidently at $U = 4.0$, which indicates it has a potential to have a long range order as $U > 3.5$. To find the accurate critical value of AFM long range order, in Fig. 2(b) we further extrapolate the finite size

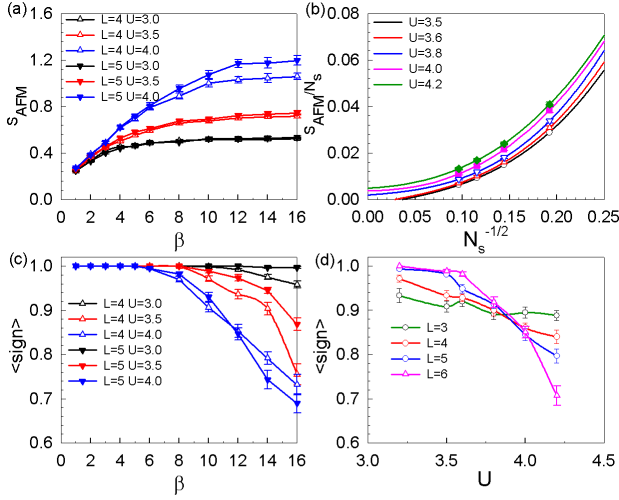


FIG. 2. (Color online) (a) The AFM spin structure factor S_{AFM} depends on $\beta = 1/T$ with different interaction strength and lattice size; (b) scaling behavior of the normalized AFM spin structure factor S_{AFM}/N_s for different values of U at $\beta = 12$. Solid lines are fit of the third-order polynomial in $1/\sqrt{N_s}$. The average of sign is shown in (c) and (d) for the simulation shown in (a) and (b) respectively.

results to the thermodynamic limit by using polynomial functions in $1/\sqrt{N_s}$, and it can be seen from the figure that the AFM long range order starts to appear around $U \simeq 3.6 \sim 3.8$, this value is very near to our previous findings $U \simeq 3.8$ on the original geometry[40].

For the finite temperature DQMC method, the notorious sign problem prevents exact results for lower temperature, higher interaction, or larger lattice for cases without particle-hole symmetry. To examine the reliability of the present data shown in Fig.2, we show the average of sign in Fig. 2(c) and (d), dependent on different temperature β at different interaction U (a) and different lattice size (b) with the Monte Carlo parameters of 30 000 times runs. For the present results, our numerical results are reliable as one can see that the average of corresponding sign is mostly larger than 0.70 for the U from 3.0 to 4.0 with 30 000 times measurements. In order to obtain the same quality of data as $\langle sign \rangle \simeq 1.0$, much longer runs are necessary to compensate the fluctuations. Indeed, we can estimate that the runs need to be stretched by a factor on the order of $\langle sign \rangle^{-2}$ [50–52]. In our simulations, some of the results are obtained with more than 240 000 times runs, and thus the results for the current parameters are reliable.

Secondly, we examine the temperature dependence dc conductivity $\sigma_{dc}(T)$ with $L = 4, 5$ across several interaction strengths, respectively, as shown in Fig 3. The conductivity is computed from the momentum \mathbf{q} and imaginary time τ dependent current correlation function [47] $\sigma_{dc}(T) = \frac{\beta^2}{\pi} \Lambda_{xx}(\mathbf{q} = 0, \tau = \beta/2)$, where $\Lambda_{xx}(\mathbf{q}, \tau) = \langle \hat{j}_x(\mathbf{q}, \tau) \hat{j}_x(-\mathbf{q}, 0) \rangle$, and $\hat{j}_x(\mathbf{q}, \tau)$ is the

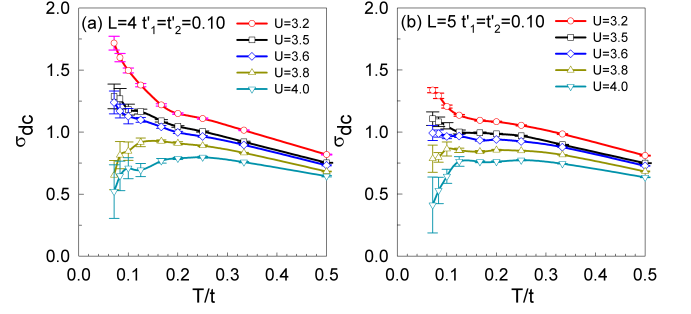


FIG. 3. (Color online) The dc conductivity σ_{dc} versus temperature T computed at various interaction strengths for (a) $L = 4$ and (b) $L = 5$.

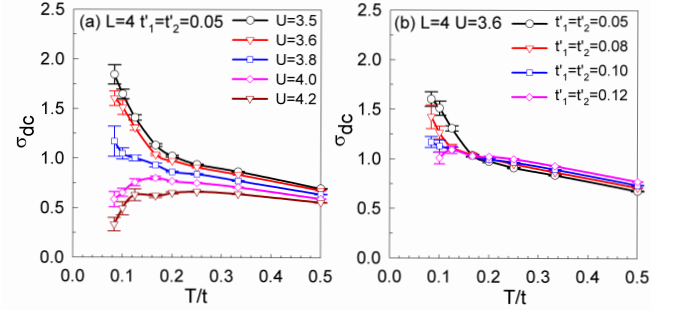


FIG. 4. (Color online) The dc conductivity σ_{dc} versus temperature T computed at (a) various interaction strengths for $t'_1 = t'_2 = 0.05$ and (b) at $U = 3.6$ for different $t'_1 = t'_2$.

current operator in the x direction. For $U < 3.6$, σ_{dc} diverges as the temperature T decreases to the zero, while the conductivity curve is concave down and closed to zero with decreasing temperature for $U \geq 3.8$. These behaviors of σ_{dc} curve in low temperature region suggest that there is a metal-insulator transition at $U \simeq 3.6 \sim 3.8$, which is nearly consistent with results obtained from the original model where the critical value $U_c \simeq 3.8$ [40]. Moreover, the critical Hubbard interaction for antiferromagnetic long range order is almost the same as that from semi-metal to antiferromagnetic insulator, which again confirms our findings that there is no spin liquid phase in magic angle twisted bilayer graphene.

In the experimental results of Ref.[3], one intriguing behavior reported is that the superconductivity is tuned by applying hydrostatic pressure. It is interesting to ask what is the fate of the correlated insulating phases by varying the interlayer coupling t'_1 and t'_2 , which may shed light on the relation between the superconducting phases and insulating phases. In Fig.4 (a), the dc conductivity σ_{dc} versus temperature T computed at various interaction strengths for $t'_1 = t'_2 = 0.05$ is shown, which indicates that the metal-insulating transition is in the region of $U_c = 3.8 \sim 4.0$, a little larger than that of $t'_1 = t'_2 = 0.10$. The dc conductivity for

different interlayer coupling at $U = 3.6$ is shown in Fig. 4 (b), which clearly show that the dc conductivity is reduced as the interlayer coupling increases, and a smaller U_c of metal-insulator transition is required for larger interlayer coupling. We also examine behavior of the spin correlation as the interlayer coupling strength varies, which show that the spin correlation is also suppressed as the interlayer coupling strength increases.

To understand the tunable superconductivity in TBG realized by varying the interlayer spacing with hydrostatic pressure, we studied the effective pairing interaction with different pairing symmetry as a function of the electronic fillings for $t'_1 = t'_2 = 0.10$ in Fig. 5.

The effective pairing interaction is defined as $\mathbf{P}_\alpha = P_\alpha - \tilde{P}_\alpha$ with

$$P_\alpha = \frac{1}{N_s} \sum_{l,i,j} \int_0^\beta d\tau \langle \Delta_{l,\alpha}^\dagger(i, \tau) \Delta_{l,\alpha}(j, 0) \rangle, \quad (5)$$

where α stands for the pairing symmetry and the corresponding order parameter reads

$$\Delta_{l,\alpha}^\dagger(i) = \sum_l f_\alpha(\delta_l) (a_{li\uparrow} b_{li+\delta_{l\downarrow}} - a_{li\downarrow} b_{li+\delta_{l\uparrow}})^\dagger, \quad (6)$$

with $f_\alpha(\delta_l)$ being the form factor of pairing function. To extract the intrinsic pairing interaction in finite system, one should subtract from P_α its uncorrelated single-particle contribution \tilde{P}_α , which is achieved by replacing $\langle a_{li\downarrow}^\dagger a_{lj\downarrow} b_{i+\delta_{l\uparrow}}^\dagger b_{j+\delta_{l\uparrow}} \rangle$ in Eq. (6) with $\langle a_{i\downarrow}^\dagger a_{j\downarrow} \rangle \langle b_{i+\delta_{l\uparrow}}^\dagger b_{j+\delta_{l\uparrow}} \rangle$.

In Fig. 5(a), it is shown that for the investigated filling region, the pairing with $d + id$ symmetry dominate over pairings with other symmetry, agree with our previous results on the original geometry[40], and the positive effective pairing interaction indicating there is indeed the possibility of electronic correlation driven superconductivity. For the exact pairing form, we refer readers to Ref.[40]. In Fig. 5 (b), the filling dependent effective pairing interaction with $d + id$ symmetry is shown for different $t'_1 = t'_2$. The effective pairing interaction with $d + id$ symmetry, P_{d+idNN} is suppressed as the interlayer coupling increases, which suggest a tunable superconductivity by varying $t'_1 = t'_2$, consistent with the experimental observation.

Summary— In summary, within an effective two orbit model for TBG, we study the spin correlation, the dc conductivity and the superconducting pairing interaction by using non-biased QMC method. At half filling, an antiferromagnetically ordered Mott insulator is proposed beyond a critical $U_c = 3.6 \sim 3.8$. By varying the interlayer coupling strength, we report a tunable metal-insulator and superconductivity in TBG, where the dc conductivity is suppressed as the interlayer coupling strength increases, and a smaller U_c for metal-insulator transition is required. With a finite doping, the pairing with $d + id$ symmetry dominates over other pairing

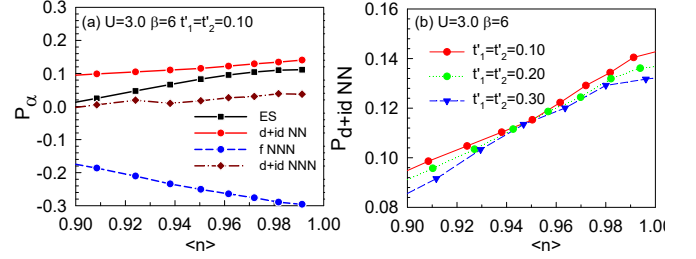


FIG. 5. (Color online) The effective pairing interaction P_α with different pairing symmetry as a function of electronic fillings for $t'_1 = t'_2 = 0.10$ (a) and the effective pairing interaction P_{d+idNN} as a function of electronic fillings for different $t'_1 = t'_2$.

symmetries, and it could be enhanced by increasing the interlayer coupling strength close to half filling. Our exact numerical results again demonstrate that the TBG holds a very similar interaction driven phase diagram of doped cuprates and other high temperature superconductors, and the TBG should be a uniquely tunable platform for exploring correlated states.

Acknowledgement — This work were supported by NSFCs (Grant. Nos. 11374034 and 11334012) and Beijing Natural Science Foundation (No. 1192011). The numerical simulations in this work were performed on HSCC of Beijing Normal University and Tianhe in Beijing Computational Science Research Center.

* txma@bnu.edu.cn

- [1] Y. Cao, V. Fatemi, A. Demir, S. Fang, S. L. Tomarken, J. Y. Luo, J. D. Sanchez-Yamagishi, K. Watanabe, T. Taniguchi, E. Kaxiras, R. C. Ashoori, and P. Jarillo-Herrero, *Nature* **556**, 43 (2018).
- [2] Y. Cao, V. Fatemi, S. Fang, K. Watanabe, T. Taniguchi, E. Kaxiras, and P. Jarillo-Herrero, *Nature* **556**, 80 (2018).
- [3] M. Yankowitz, S. Chen, H. Polshyn, Y. Zhang, K. Watanabe, T. Taniguchi, D. Graf, A. F. Young, and C. R. Dean, *Science* (2019), 10.1126/science.aav1910.
- [4] J. G. Bednorz and K. A. Muller, *Z. Phys. B* **64**, 189 (1986).
- [5] F. Steglich, J. Aarts, C. D. Bredl, W. Lieke, D. Meschede, W. Franz, and H. Schafer, *Phys. Rev. Lett.* **43**, 1892 (1979).
- [6] Y. Kamihara, T. Watanabe, M. Hirano, and H. Hosono, *J. Am. Chem. Soc.* **130**, 3296 (2008).
- [7] D. Jerome, A. Mazaud, M. Ribault, and K. Bechgaard, *J. Phys. Lett. (Paris)* **41**, 95 (1980).
- [8] D. J. Scalapino, *Rev. Mod. Phys.* **84**, 1383 (2012).
- [9] C. Xu and L. Balents, *Phys. Rev. Lett.* **121**, 087001 (2018).
- [10] B. Roy and V. Juricic, *arXiv:1803.11190*.
- [11] G. Baskaran, *arXiv:1804.00627*.
- [12] J. F. Dodaro, S. A. Kivelson, Y. Schattner, X. Q. Sun, and C. Wang, *Phys. Rev. B* **98**, 075154 (2018).

- [13] A. Ramires and J. L. Lado, *Phys. Rev. Lett.* **121**, 146801 (2018).
- [14] Y. Cao, D. Chowdhury, D. Rodan-Legrain, O. Rubies-Bigordà, K. Watanabe, T. Taniguchi, T. Senthil, and P. Jarillo-Herrero, [arXiv:1901.03710](#) (2019).
- [15] G. Chen, L. Jiang, S. Wu, B. Lv, H. Li, K. Watanabe, T. Taniguchi, Z. Shi, Y. Zhang, and F. Wang, [arXiv:1803.01985](#) (2018).
- [16] C. Xu and L. Balents, *Phys. Rev. Lett.* **121**, 087001 (2018).
- [17] N. F. Q. Yuan and L. Fu, *Phys. Rev. B* **98**, 045103 (2018).
- [18] N. F. Q. Yuan and L. Fu, *Phys. Rev. B* **98**, 079901 (2018).
- [19] H. C. Po, L. Zou, A. Vishwanath, and T. Senthil, *Phys. Rev. X* **8**, 031089 (2018).
- [20] H. C. Po, L. Zou, T. Senthil, and A. Vishwanath, [arXiv:1808.02482](#) (2018).
- [21] C.-C. Liu, L.-D. Zhang, W.-Q. Chen, and F. Yang, *Phys. Rev. Lett.* **121**, 217001 (2018).
- [22] J. F. Dodaro, S. A. Kivelson, Y. Schattner, X. Q. Sun, and C. Wang, *Phys. Rev. B* **98**, 075154 (2018).
- [23] X. Y. Xu, K. T. Law, and P. A. Lee, *Phys. Rev. B* **98**, 121406 (2018).
- [24] Y.-H. Zhang, D. Mao, Y. Cao, P. Jarillo-Herrero, and T. Senthil, [arXiv:1805.08232](#) .
- [25] M. Koshino, N. F. Q. Yuan, T. Koretsune, M. Ochi, K. Kuroki, and L. Fu, *Phys. Rev. X* **8**, 031087 (2018).
- [26] F. Wu, A. H. MacDonald, and I. Martin, *Phys. Rev. Lett.* **121**, 257001 (2018).
- [27] Q. Tang, L. Yang, D. Wang, F. Zhang, and Q. Wang, [arXiv:1809.06772](#) (2018).
- [28] L. Zou, H. C. Po, A. Vishwanath, and T. Senthil, *Phys. Rev. B* **98**, 085435 (2018).
- [29] J. Kang and O. Vafek, *Phys. Rev. X* **8**, 031088 (2018).
- [30] A. Thomson, S. Chatterjee, S. Sachdev, and M. S. Scheurer, *Phys. Rev. B* **98**, 075109 (2018).
- [31] J. W. F. Venderbos and R. M. Fernandes, *Phys. Rev. B* **98**, 245103 (2018).
- [32] G.-Y. Zhu, T. Xiang, and G.-M. Zhang, *Science Bulletin* **63**, 1087 (2018).
- [33] L. Zhang, [arXiv:1804.09047](#) (2018).
- [34] Y.-Z. You and A. Vishwanath, [arXiv:1805.06867](#) (2018).
- [35] B. Lian, Z. Wang, and B. A. Bernevig, [arXiv:1807.04382](#) (2018).
- [36] Z. Song, Z. Wang, W. Shi, G. Li, C. Fang, and B. A. Bernevig, [arXiv:1807.10676](#) (2018).
- [37] J. Liu, J. Liu, and X. Dai, [arXiv:1810.03103](#) (2018).
- [38] M. Xie and A. H. MacDonald, [arXiv:1812.04213](#) (2018).
- [39] Z. Zhu, D. Sheng, and L. Fu, [arXiv:1812.05661](#) (2018).
- [40] T. Huang, L. Zhang, and T. Ma, [arXiv:1804.06096](#) (2018), <https://doi.org/10.1016/j.scib.2019.01.026>.
- [41] A. Kerelsky, L. McGilly, D. M. Kennes, L. Xian, M. Yankowitz, S. Chen, K. Watanabe, T. Taniguchi, J. Hone, C. Dean, *et al.*, [arXiv:1812.08776](#) (2018).
- [42] Y. Choi, J. Kemmer, Y. Peng, A. Thomson, H. Arora, R. Polski, Y. Zhang, H. Ren, J. Alicea, G. Refael, *et al.*, [arXiv:1901.02997](#) (2019).
- [43] Y. Otsuka, S. Yunoki, and S. Sorella, *Phys. Rev. X* **6**, 011029 (2016).
- [44] T. Ma, Z. Huang, F. Hu, and H.-Q. Lin, *Phys. Rev. B* **84**, 121410 (2011).
- [45] T. Ma, F. Yang, H. Yao, and H.-Q. Lin, *Phys. Rev. B* **90**, 245114 (2014).
- [46] T. Ma, F. Hu, Z. Huang, and H.-Q. Lin, *Applied Physics Letters* **97**, 112504 (2010).
- [47] N. Trivedi and M. Randeria, *Phys. Rev. Lett.* **75**, 312 (1995).
- [48] P. J. H. Denteneer, R. T. Scalettar, and N. Trivedi, *Phys. Rev. Lett.* **83**, 4610 (1999).
- [49] T. Ma, L. Zhang, C.-C. Chang, H.-H. Hung, and R. T. Scalettar, *Phys. Rev. Lett.* **120**, 116601 (2018).
- [50] R. Blankenbecler, D. J. Scalapino, and R. L. Sugar, *Phys. Rev. D* **24**, 2278 (1981).
- [51] R. R. d. Santos, *Brazilian Journal of Physics* **33**, 36 (2003).
- [52] G. Yang, S. Xu, W. Zhang, T. Ma, and C. Wu, *Phys. Rev. B* **94**, 075106 (2016).